Mars Ground Level Enhancements in the Context of the Solar Energetic Particle Clock

Arik Posner [1,2], Ian. G. Richardson[3,4], Cary Zeitlin[2,5]

1: NASA HQ, SMD/Heliophysics Division, Washington DC 20546

2: NASA JSC, SMOD/Space Radiation Analysis Group, Houston TX, 77058

3: Univ. Maryland, Dept. Astronomy, College Park, MD 20742

4: NASA GSFC, Heliophysics Science Division, Greenbelt, MD 20771

5: KBR Wyle Services LLC, Houston, TX 77002

In this work we discuss the growing ensemble of solar energetic particle events registered on the Martian surface, including their temporal appearance and solar sources. Solar energetic particle events have been observed from the surface of Mars since soon after the August 2012 landing of the Radiation Assessment Detector onboard Curiosity. The Martian atmosphere prevents protons and heavy ions of up to 180 MeV/n kinetic energy from directly reaching the Martian surface. This cut-off is high enough to limit the number of solar energetic particle events measured on the surface to only 15 in ~12 ½ years. Yet we find in this analysis that Mars ground level enhancements follow the distinct SEP clock pattern for proton events observed at lower energies as reported in Posner, Richardson, and Strauss (2024). Proton acceleration occurs predominantly near the solar surface, while transport to Mars incurs a delay in onset, and, as we show here, peak intensity. These delays are a function of the longitudinal magnetic connection distance. between the foot point of solar wind magnetic field lines that intersect the Mars environment with the source longitude of the solar magnetic eruption. A distinct clustering of solar source locations at or near the Mars foot points at the Sun's western limb relative to Mars is apparent, indicating lower flux thresholds from such preferred locations. Our findings have implications for astronaut safety at Mars.

1 Introduction

On August 5, 2012, Curiosity arrived on the surface of Mars. Soon thereafter, the Radiation Assessment Detector (RAD) began observations of the ground-level ionizing radiation environment. For more than eight months, the surface radiation environment was dominated by galactic cosmic rays and their secondary particles generated in the interaction with the atmosphere and the ground (Ehresmann et al., 2014). Only on April 11, 2013, did the typical pattern of a solar energetic particle event, a sudden rise and slow decay in the radiation intensity, become evident in RAD observations on the Martian surface. This first Mars Ground Level Enhancement (MGLE) was also observed as a solar particle event at different locations around the Sun (see, e.g., Hassler et al., 2014) , from particle instruments on the Solar and Heliospheric Observatory (SOHO, Domingo, Fleck & Poland, 1995) and STEREO A and B (Kaiser et al., 2008). Figure 1 shows the relative locations of Earth, Mars, and the STEREO s/c.

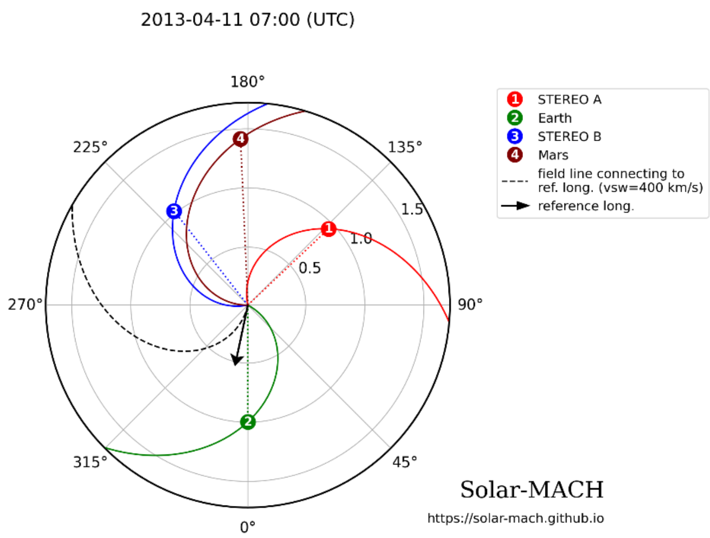

Figure 1. Inner-heliosphere locations of STEREO A (1), Earth (2), STEREO B (3), and Mars (4) with respect to the Sun (center) and the longitude of the associated solar flare (arrow, see Table 1) during the first observed Mars Ground Level enhancement of Apr. 11, 2013. View is from north of the ecliptic plane. Nominal Parker magnetic field lines indicate the approximate magnetic connectivity to the Sun.

Wide-spread events observed in space have been known since 1970 (Dodson-Prince et al., 1977). A more recent systematic study of wide-spread solar particle events by Richardson et al. (2014) used observations from three s/c at ~ 1 AU (STEREO A, B, SOHO). This study commencing with the launch of STEREO s/c in October 2006 included the identification of all solar source locations, aided by direct flare observations and also considering the kinematics of coronal mass ejections in coronagraph imagery. They found the source region related to this event to be an active region near Earth's subsolar point, just 12° east of the central meridian. As viewed from Earth, only one week later, on April 18, 2013, Mars passed its conjunction with the Sun, meaning Mars was located almost directly on the opposite side of the Sun from the solar activity that caused the April 11 MGLE as shown in Figure 1, where the arrow indicates the longitude of the flare. The STEREO spacecraft were located on either side of Mars as viewed from Earth, separated by 130° (STEREO B) and -146° (STEREO A) in terms of solar longitude from the flare location, and both also recorded the particle event. These early observations suggest a connection between MGLEs and wide-spread solar energetic particle events. The comprehensive list of SEP events including such wide-spread events by Richardson et al. (2014) has been extended to 2023 at the time of writing, and made available to the public (Richardson, 2024). The list contains a total of 245 individual 1 AU proton events at ~25 MeV in the period Aug. 2012 – Nov. 2023, and includes all 8 MGLEs observed during this period, suggesting that MGLEs are a subset of extreme SEP events that are usually observed over extended regions of the inner heliosphere. Since then, seven additional MGLEs have occurred as activity ramps up during the approach to the peak of solar cycle 25, bringing the total to 15. The dates of MGLEs # 1 – 15 together with other parameters to be discussed below, are listed in Table 1.

A number of studies have addressed MGLEs so far: Aspects of individual MGLEs, including dose rate and dose equivalent rate on the Martian surface, have been discussed by various authors. Guo et al. (2015) discuss the implications for entire human exploration missions, including round trip periods. The intense September 10, 2017 MGLE (#6 in our Table 1) allowed Zeitlin et al. (2018) to discuss for the first time the identification of primary SEP protons and their impact on dose rate on the Martian surface. Moreover, Guo et al. (2018) discussed the same event regarding the solar/heliospheric origins in a global CME shock scenario. They found that the observed CME's shock would have reached the magnetic field line Mars was on at or near the onset of the MGLE too late to explain the observed particle arrival and suggest that particle cross-field transport in the heliosphere may be required They further suggest that a stream interaction region (SIR) may have aided the trapping and re-acceleration of CME-shock accelerated particles, resulting in the MGLE. Bruno et al. (2019) discuss observations of this and other SEP events in September 2017 measured at Earth and STEREO A in the context of their solar sources and solar wind structures. Guo et al. (2019a) discuss a larger ensemble of MGLEs. This work treats MGLEs up to MGLE #6 (by omitting #5, up to Sept. 10, 2017), again, in terms of overall dose rate.

The particular focus of this work is to study the solar sources of MGLEs and to test predictions from the "SEP clock" (Posner, Richardson & Strauss, 2024, hereafter PRS24) that may apply to MGLEs. Theoretically, as CME shocks expand into the heliosphere, they would reduce the length of the direct magnetic field connection between the shock and the observer (Wijsen et al., 2022), thus reducing the path length and therefore shortening the duration of proton energy dispersion. PRS24, however, find that the shortest path lengths are found in well-connected events, with systematically increasing path lengths as the magnetic connection worsens. Therefore, the study suggests both a dominant role of particle cross-field transport and a reduced role of CME-driven shocks regarding the appearance of solar particle events.

It is the purpose of this study to explore links between the "SEP clock" picture drawn above and solar particle events observed on the Martian surface. If the dominance of cross-field diffusion applies to those high-energy protons that give rise to MGLEs, solar source longitudes can lie very far away from the nominal magnetic field connection of Mars at the Sun. Overall weaker events would be more likely to originate from near the nominal magnetic connection longitude, which is ~W90 relative to Mars (see Table 1 in Posner et al., 2021). Moreover, poorly-connected events would be expected to show a delay in onset time and possibly a slower rate of increase than well-connected events owing to the slow unfolding of the cross-field transport process.

In a CME-driven shock scenario, onset delays of MGLEs would also be expected, presumably larger than those in the SEP clock picture, but as the shock approaches Mars, the duration of energy dispersion would shorten, and the intensity rise would be more rapid for events that are not well connected. In addition, a shift towards solar source regions closer to the central meridian relative to Mars should be observed, as CMEs originating from these regions would be most likely to encounter Mars.

The following section describes the underlying observations. Section 3 tests these two pictures against the observations. In Section 4 we address new insights into MGLE forecasting. Section 5 summarizes our work,

2 Observations

The Radiation Assessment Detector (RAD) onboard Curiosity owes its heritage to a compact design for a space-based solar energetic electron and ion detector system that is also capable of detecting neutrons. It was originally intended for the Solar Orbiter mission, as described in Posner et al. (2006). In the same year, a variant of the instrument intended for Mars surface operations was created with modifications to make it suitable for the Mars Science Laboratory, now Curiosity. Curiosity was launched in November 2011 and landed in Gale crater on Mars in August 2012. At this location, the Martian (mostly CO_2)

atmosphere with a surface pressure of ~730 Pa shields against most low-energy energetic charged particles. Protons require a minimum of ~180 MeV to reach the surface, while heavy ions have even higher MeV/n thresholds. The penetration depth varies over the course of a Martian day, or Sol, as the pressure changes in a diurnal cycle have a direct measurable effect on cosmic ray surface dose rates (Rafkin et al., 2013).

The RAD instrument, fully described in Hassler et al. (2012), can detect primary particles from space and secondary particles generated by the interaction of high-energy cosmic rays with the atmosphere, including protons and heavy ions, electrons, neutrons, X- and gamma rays, muons and pions. This work analyzes total surface dose rate data publicly available from the SPDF. The two types of dose rates used here are from the solid-state detector “B” that measures charged particles, and from the plastic scintillator detector system “E” that is sensitive to both charged and neutral ionizing radiation. Detector “E” is located deeper in the instrument and is partially shielded from above by a significant CsI scintillator that can stop protons of up to ~100 MeV. The time resolution of the publicly available RAD data is variable and changes over time, within the range of 7 minutes to below two hours.

3 Mars Ground Level Enhancements 2012 – 2024 and the SEP Clock

A total of fifteen MGLEs have been observed between August 2012 and December 2024. Figure 1 shows observed dose rates over the course of two (Earth) days for the three most intense MGLEs. Here, the top graph shows dose rates of detector “B”, i.e., predominantly charged primary and secondary particles. For comparison, the bottom graph shows dose rates recorded in detector “E” that include contributions from secondary neutrons and also charged particles but observed at a higher shielding depth. Overall, there are minor differences between the top and bottom graphs. After subtraction of the pre-event GCR-based dose rate, twelve of the 15 MGLEs have higher peak dose rates in the lower-shielded “B” detector. However, notably, the most intense event (MGLE #9) is one of a subset of events in which the peak dose rate is higher in the more heavily shielded "E" detector. In this case, the peak does in "E" is ~15% higher than recorded in "B".

In terms of overall observed peak dose rate, the MGLEs remain far below thresholds that may lead to acute radiation sickness (Kim, Hu & Cucinotta, 2005). The strongest event, MGLE #9, increased the surface dose rate by a record 4900%. For comparison, this event is equivalent in terms of increase over pre-event background to the most intense Earth Ground Level Enhancement on Feb. 23 1956 (see, e.g., the Ground Level Enhancement database at https://gle.oulu.fi/#/). The event arose from AR13664, the same active region complex that caused a significant geomagnetic storm at Earth on May 10, then rotated behind the limb. The X-ray flare associated with the May 20, 2024 eruption was observed directly by Solar Orbiter, and estimated to be X16.5. From Mars’ point of view, the solar event occurred in the Sun’s far western hemisphere (W71). Mars was near perihelion, at ~1.38AU distance from the Sun, marking the closest Mars-Sun distance during any of the 15 MGLEs. It was thus apparently well connected with Mars via the interplanetary magnetic field. Overall, given the extreme flare, the proximity and good nominal magnetic field connectivity with the source region, this MGLE may represent a near worst-case scenario in terms of radiation exposure from solar particles and their secondaries on the Martian surface. The event was recorded as a solar particle event in near-Earth space by SOHO and STEREO-A, but at a moderate intensity owing to the poor magnetic connection conditions.

All MGLEs have dose-time profiles that are typical of high energy SEP events in the heliosphere, with a more rapid rise than decline phase. A second enhancement from the arrival of an interplanetary shock at Mars, the “energetic storm particle” (ESP) component, often observed in space, has not been observed on the surface of Mars as might be expected due to the high atmospheric cut off since ESP events are most prominent at low energies and only occasionally exceed 40 MeV in protons (Lario et al., 2023).

The number of MGLEs is far below the number of solar energetic proton events observed in this time period from a single or multiple inner-heliosphere spacecraft (SOHO, STEREO). For example, the list of Richardson (2024) contains a total of 245 solar energetic proton enhancements at ~25 MeV in the period Aug. 2012 – Nov. 2023. Notably, each of the first 8 MGLEs, occurring when the STEREO spacecraft were still well-separated from Earth, was observed at ~25 MeV by each of the active s/c, suggesting that the solar particle events that gave rise to MGLEs were generally observed all around the Sun. The remaining seven MGLEs occurred in 2024, during the rise phase of Solar Cycle 25. All these events were associated with SEP events observed at Solar Orbiter, STEREO A and SOHO, with the exception of event 13 which was not evident at STEREO A and only a weak event was observed by SOHO.

The ratio of ~25 MeV proton events at 1 AU to MGLEs in overlapping time periods of the two lists so far is on the order of 30:1. It remains to be seen whether this ratio is dependent on the overall strength of the solar cycle. Several authors have shown that solar cycle 24 was unusually weak- as compared to previous cycles, in terms of sunspot number (Javaraiah, 2024), X ray flares (Pandey et al., 2023), and also GLEs at Earth.

All 15 MGLEs have been analyzed to determine their onset time. We use a similar method as Posner, Richardson & Strauss (2024). Red vertical lines in Fig. 1 indicate the times of onsets of type-III radio bursts associated with the solar activity that gave rise to each event. Type-III radio bursts are associated with the escape of suprathermal or energetic electrons from the Sun, where their spectrum can give rise to Langmuir waves and radio emission at the local plasma frequency and its harmonic. They typically start at high frequencies in the corona (~GHz) and drift quickly to low frequencies, even occasionally to the local plasma frequency, i.e. to tens of kHz near 1 AU.

We use observations of type-III radio bursts by the WAVES instrument (Bougeret et al., 1995) on Wind (Ogilvie & Parks, 1996) at Earth/Sun L1 and from S/WAVES (Bougeret et al., 2008) on the STEREO spacecraft, where these data are available. Blue vertical lines in Figure 2 bound the time intervals when least squares fits are made to the logarithm of the (exponential) dose rate increases in the B or E detectors to derive two onset times for each event. Each individual onset time is determined as the time when the exponential fit intersects with the average pre-event (pre-type-III onset) dose rate measured in the four hours leading up to the event (indicated as a blue horizontal line). The average of the “B”-detector and “E”-detector onset times is entered as the “SEP onset” in Table 1. We define the error in onset time determination as either the distance of the individual onset times from the average, or the instrumental time resolution, whichever is larger. The onset delay is determined as the difference between the onset time of the MGLE and the solar release time of the associated type-III radio burst, i.e., 8 min before the onset of the type III at Wind or STEREO at 1 AU.

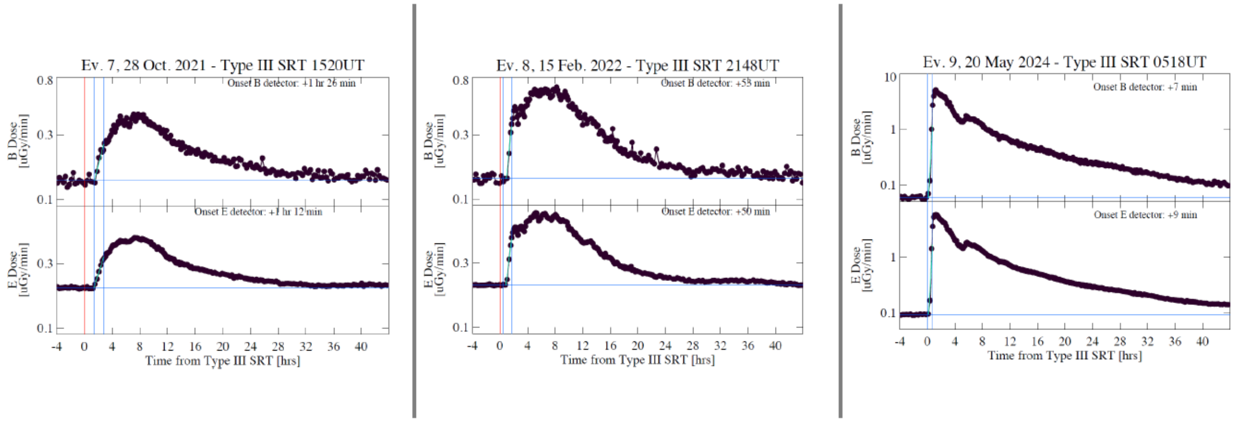

Figure 2. Mars Ground Level Enhancements 7-9, observed on Oct. 8, 2021, Feb. 15, 2022, and May 20, 2024, respectively. For each event we display two days of dose rates measured by detector "B" (top graph) and detector "E" (bottom graph).. Onset time delays of the MGLE observations with respect to the type-III radio burst onsets are included at the top of each graph. The methodology of onset determination is discussed in the main text.

Table 1 lists each of the events and their derived onset times in temporal order. The list contains event date, type-III radio burst and MGLE onset times, their respective delays, and flare information, including GOES soft X-ray brightness (where available), and locations (directly observed and inferred as collated in Richardson, 2024) until the end of 2023. Soft X-ray flare brightnesses in parenthesis are estimates from Solar Orbiter. Any more recent flare information is taken from the public Community Coordinated Modeling Center (CCMC) Space Weather Database Of Notifications, Knowledge, Information (DONKI) at https://kauai.ccmc.gsfc.nasa.gov/DONKI. Approximate Mars magnetic field foot point locations at the Sun are inferred from back mapping to the Sun using an ideal Parker spiral field line that intersects Mars' location and assumes a constant solar wind speed. In cases where upstream solar wind observations from the Mars Atmosphere and Volatile EvolutioN (MAVEN) spacecraft (Jakosky et al., 2015) are available within 24 hours of type-III radio burst onset, they are used. Halekas et al. (2017) discuss how to infer solar wind speeds from MAVEN/SWIA and MAG data. Where not available, we use the average solar wind speeds observed by MAVEN in the same calendar year, or, if recorded before 2014, of the calendar year nearest to the observation.

"Clock angles" for the flare source longitude relative to Mars are defined in a similar way as in PRS2024 with Mars assumed to be fixed at clock hour "6". Note that the magnetic connection distances are angular distances of Mars' inferred magnetic field foot point from the (actual or inferred) flare location. Therefore, they differ from clock angle.

Maximum dose rates for MGLEs from the "B" and "E" detectors are determined as the maxima observed during the event with the pre-event (pre-type-III radio burst) galactic cosmic ray-induced background subtracted (see above). The dataset available to the public already has background from the on-board RTG power source subtracted. Peak delays of MGLEs are also calculated also with respect to the solar release time of the associated type-III radio burst.

The first six MGLEs occurred during the latter half of solar cycle 24, while the remaining nine MGLEs are related to solar activity in the more active cycle 25. Each of the first three cycle-25 events (MGLEs 7-9, Figure 2) at the time set a new peak dose rate record in both the "B" and "E" detectors. Notably, the most recent seven events occurred within a time span of ~6 months. As also found for each of the “SEP clock” study’s SEPs of PRS24, each of the 15 MGLEs is associated with one type-III radio burst or a series of type-III radio bursts. Note that type-III radio bursts are useful in several ways: In contrast to solar flares that are not visible if occurring off the limb and on the far side, at ~1 MHz they provide a reliable time marker observable from any solar longitude of all significant solar energetic particle events. They are potentially obstructed at high frequencies by the limb of the Sun or high-density near-Sun solar wind for far side events relative to the observer. However, at frequencies at or just below 1 MHz, type-III radio bursts always precede SEP arrival, even the arrival of the SEP’s relativistic electrons (Posner et al., 2024), which were recognized as the first in-situ sign of a solar particle event by Van Hollebeke, Ma Sung & McDonald (1975). Furthermore, they set a time marker for pre-SEP-event background determination, including MGLEs as shown above. In addition, the time marker set by the type-III burst onset also is a good proxy for determining SEP (proton, electron) arrival time delays, also described above.

Table 1. List of all 15 Mars Ground Level enhancements 2012 – 2024 observed by Curiosity/RAD and their associated solar phenomena.

No.	Date	Type III Obs. Onset, Sol. Rel. Time [UT]	SEP Onset Mars [UT]	Delay wrt SRT [min]	Flare Loc. Wrt Mars [°], Clock hr.	MVN Vsw* [km/s]	Mars Dist. Wrt Sun [AU] Day/ Nght	Mars FP, Flare Conn. Dist. [°], Magn.	Max Dose Rate B [μGy/ hr]	Max Dose Rate E [μGy/ hr]	Max Del. B vs SRT [min]	Max Del. E vs SRT [min]
1 (20)	11 Apr. 2013	06:58 06:50	06:50	60 ±123	W165 **12**/1	*409*	1.42 Nght	W85.3 79.7 M6.5	3.0	2.1	357 ±123	479 ±123
2 (29)	11 Oct. 2013	07:14 07:06	07:50	44 ±9	W162 1	*409*	1.63 Nght	W98.0 64.0 (M1.5)	8.9	8.0	215 ±9	224 ±13
3 (34)	6 Jan. 2014	07:46 07:38	10:05	147 ±50	W59 4	*409*	1.67 Nght	W100.4 -41.4	4.3	2.0	282 ±34	315 ±34
4 (46)	1 Sept. 2014	11:01 10:53	16:59	366 ±58	E43 **7**	*409*	1.45 Day	W87.1 -130.1	5.3	5.0	1163 ±9	1333 ±9
5 (50)	29 Oct. 2015	02:17 02:09	03:57	108 ±30	E15 **6**/7	*404*	1.66 Nght	W101.0 -116.0	1.2	0.9	260 ±23	237 ±23
6	10 Sept. 2017	15:55 15:47	20:25	278 ±9	E68 **8**	400	1.66 Nght	W102.0 170.0 X8.2	15.3	13.4	1061 ±9	878 ±9
7	28 Oct. 2021	15:28 15:20	16:44	84 ±9	W164 **1**	377	1.61 Nght	W105.0 59.0 X1.0	17.3	15.9	425 ±9	434 ±9
8	15 Feb. 2022	21:56 21:48	22:39	51 ±9	W89 **3**	*435*	1.48 Nght	W83.6 5.4	31.9	29.8	493 ±9	311 ±9
9	20 May 2024	05:15 05:07	05:15	8 ±9	W71 **4**	*380*	1.38 Day	W89.3 -18.3 (X16.5)	300.1	343.5	72 ±9	72 ±9

10	22 Jul. 2024	(23:56) (23:48)	00:25 (+1d)	37 ±17	W83 3	*380*	1.42 Day	W91.8 -8.8 (X14)	8.2	7.9	214 ±17	214 ±17
11	05 Aug. 2024	13:37 13:29	13:22	-7 ±17	W21 **5**	*380*	1.43 Day	W92.5 -71.5 (X1.7)	1.6	1.5 (spike)	165 ±17	114 ±17
12	3 Sept. 2024	07:48 07:40	08:22	42 ±17	W87 3	*380*	1.47 Day	W95.1 -8.1	3.7	2.1	126 ±17	144 ±17
13	5 Sept. 2024	07:04 06:56	07:19	23 ±17	W105 **2**/3	337	1.47 Day	W107.2 -2.2	5.5	5.8	99 ±17	99 ±17
14	9 Oct. 2024	01:48 01:40	03:27	107 ±21	E44 7	444	1.51 Day	W83.6 127.6	1.8	1.4	1024 ±17	570 ±17
15	21 Nov. 2024	1800 1752	1812	20 ±17	W90 3	*380*	1.57 Nght	W101.6 -11.6	4.2	4.4	84 ±17	135 ±17

Figure 3 uses the clock angle information of Table 1 to display the most intense MGLEs in any of the respective clock sectors where available. The scaling on all MGLEs that are shown is identical to allow a direct comparison of dose rates. There is one exception, MGLE #9 (also shown in Fig. 2) at the clock hour "4". Here the scale had to be compressed by a factor of 7 due to the much higher maximum dose rate for this event.

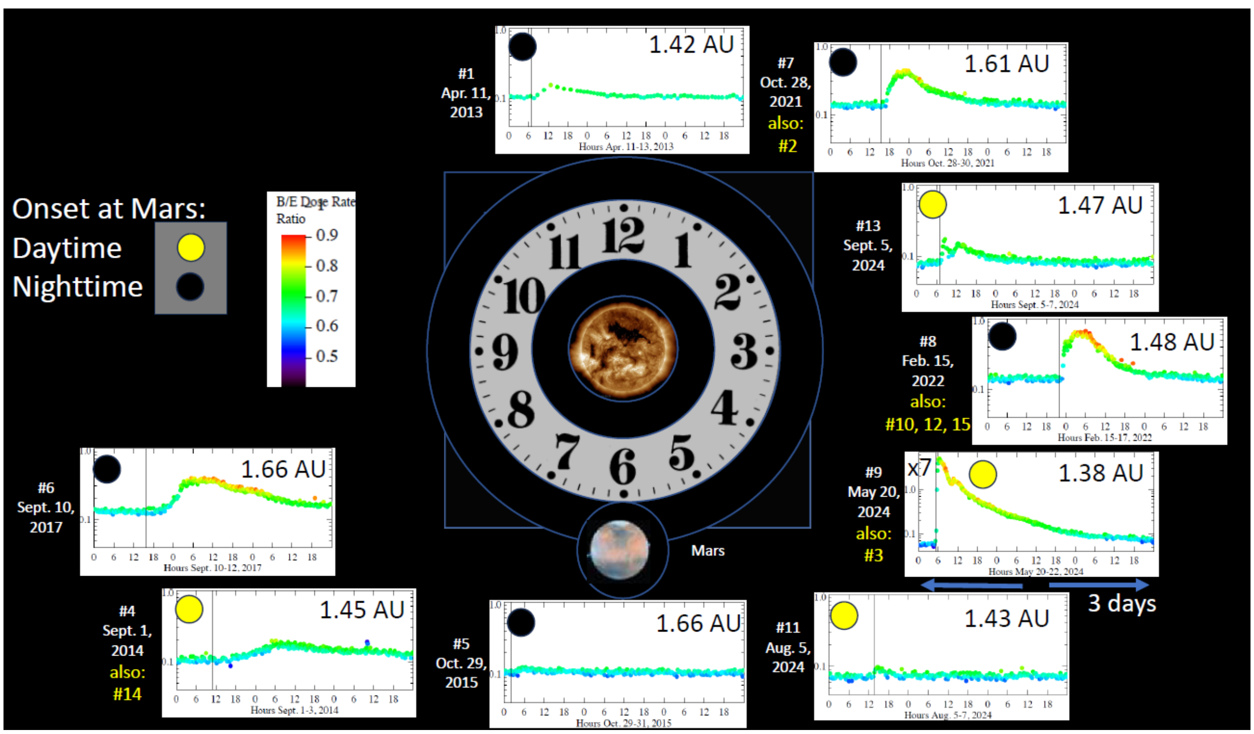

Figure 3. The Mars Ground Level Enhancement clock. The figure shows highest dose rate Mars Ground Level Enhancement for each solar clock angle source location, where available. Other events in each sector are also noted (yellow). Details are described in the text.

The individual events in Figure 3 show dose rates in detector “B”. The color represents the “B” to “E” dose rate ratio (see color scale), with relatively higher ratios indicating the presence of SEP protons that are less likely to reach the better-shielded detector “E”. Large MGLEs show clear evidence of softening of the spectrum (i.e., larger B/E ratios) in the post-peak phase of the event, whereas earlier phases, usually associated with harder spectra, do not.

Each event shown includes an indicator of day- vs. nighttime on Mars. This shows whether Curiosity observed the MGLE onset at day or night and is determined by reading off the sensor temperature, which is a function of the ambient temperature, since Mars undergoes significant temperature swings between day- and nighttime. Of the 15 MGLEs so far, eight have been observed to start during nighttime, vs seven during daytime when there can be effects on the atmospheric density and cosmic ray intensity (Rafkin et al., 2013). Sol time appears to have limited-to-no effect on MGLE onsets. Effects on dose rates over the unfolding of the event also seem to be of secondary importance, with possible small hints of modulation with a 24.5-hour (i.e., Sol) periodicity during MGLE declining phases. Several events have long-lasting decays of intensity, and, while a minor effect of modulation can be seen, the overall effect on this analysis is negligible.

Figure 3 shows that the preferential MGLE solar source longitude is near the west limb. Also including events in Table 1 that are not shown in Figure 2, a single clock hour, hour 3, is source of 27% of all events (MGLEs, #8, 10, 12, 15 – the six events not explicitly shown in Figure 2 are identified by number near the lower left side of each clock sector’s panel). This sector only represents ~8% of all solar source longitudes No events so far have originated from clock hours 9-11 that cover 25% of solar source longitudes. and correspond to sources far behind the east limb with respect to Mars. Given the low event statistics, it is not possible to rule out that future MGLEs may originate in these sectors, as is the case for lower energy SEP events (e.g., Richardson et al., 2014, PRS24). All other clock hours are sources for either a single or two MGLEs. We conclude that all source longitudes are potential sources of MGLEs, provided the overall event is extreme. The relatively more frequent moderate SEP events can only be observed as MGLEs if they originate from a preferred solar source longitudes near the W limb.

The broad range of MGLE source regions described above is in general agreement with the PRS24 SEP clock picture of particle events observed in space near 1 AU, in which cross-field diffusion appears to be the mechanism that allows SEPs to be detected very broadly in longitude. In the absence of cross-field transport, it would be difficult to explain how solar source regions of events #1, 4, 6, and 14 in the 7, 8, and 12 clock sectors can possibly give rise to the observed events. Excluding cross-field transport as a mechanism, particles accelerated to high energies by CME shocks that expand into the heliosphere would require these shocks to “touch” field lines that directly connect with Mars. However, assuming nominal Parker spiral fields, this scenario is unlikely to be consistent with the short delays between type III and MGLE onsets. Note that Guo et al (2018) find the onset of MGLE #6 to be earlier than expected from a no-cross-field transport point of view.

There is a direct overlap of wide-spread particle events listed in PRS24 with our list of MGLEs: MGLE 1 – 5 of this study are also listed as events #20, 29, 34, 46, and 50 of PRS24 (these event numbers are included in Table 1, first column, in parentheses). PRS24 analyzed proton energy dispersion, i.e., the difference in arrival times at the observing spacecraft for protons of different specified energies. They found a systematic dependence of proton energy dispersion on solar source longitude.

Of the five overlapping SEP/MGLEs of PRS24 and this work, PRS24 found that event #29 (MGLE #2) was too faint at Earth-Sun L1 and the pre-event particle background was too intense to analyze the energy dispersion duration. PRS24 event #34 (MGLE #3) cannot be used either for comparison with this study due to a SOHO energetic particle data gap during the onset at 45 MeV. However, the remaining three PRS24 events were fully analyzed for energy dispersion and provide data for the onset time delay at 45 MeV. Therefore, they can be used as a comparison with our study.

By analogy, we test whether the MGLE onset delay can be used to predict MGLE energy dispersion durations. Figure 4 shows all analyzed events of PRS24 in terms of duration of energy dispersion for protons of 45 – 10 MeV and 45 – 4.5 MeV measured at Earth by SOHO. These are displayed over the 45 MeV proton onset delay vs the type-III radio burst. We find that there is a clear correlation between onset delay and energy dispersion duration overall. This behavior is predicted if the main cause for wide spread of SEPs in the heliosphere is cross-field diffusion: 45 MeV protons are faster to diffuse across field lines than slower-moving 10 MeV or even 4.5 MeV protons. In the CME shock picture with no cross-field diffusion allowed, one would expect the opposite: The higher a CME shock expanding away from the solar surface is before connecting to the field line that connects Mars with the Sun, the shorter (on average) the remaining magnetic path length between this "connection to the observer" (COB) point and the observer at Mars would become (see Wijsen et al., 2022). Therefore, the comparatively slow CME shock propagation should have a dominant effect on onset delay, and the dispersion duration between two fixed proton energies should be anticorrelated with the onset delay. Figure 4 shows that there is a clear positive correlation between onset delay and energy dispersion duration for Earth/SOHO, favoring the cross-field diffusion picture.

The color scale used for Figure 4 relates to symbol color and shows that typically events with large magnetic connection distance have both large onset delays and large proton energy dispersion durations. Figure 4 identifies the three common events between PRS24 and this study. Their distribution fits into the above picture and confirms that SEPs that give rise to MGLEs have rather typical 4.5 – 45 MeV proton onsets at Earth/SOHO .

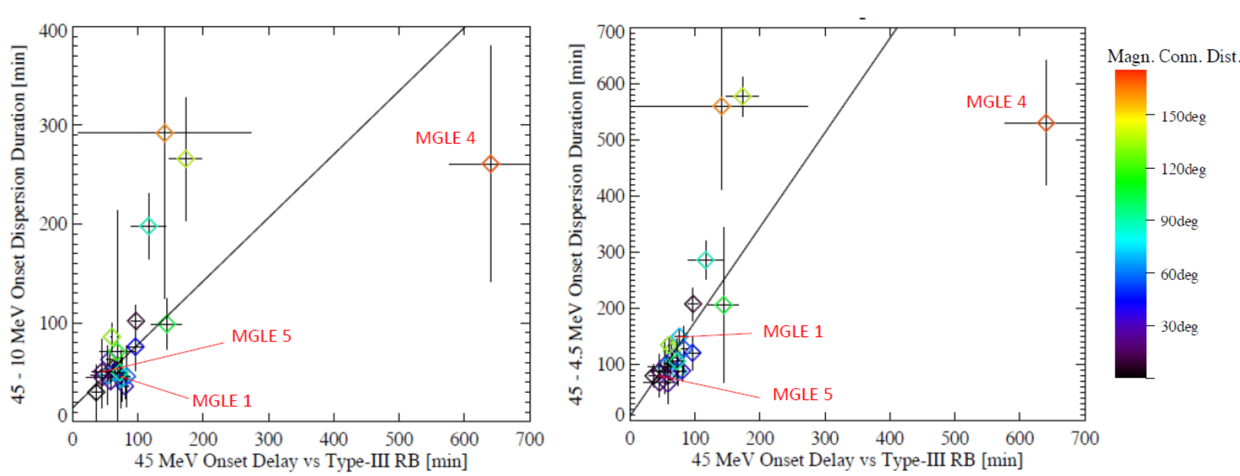

Figure 4: The figures display energy dispersion durations from onsets of wide-spread solar energetic particle events of the STEREO era. These durations, derived for 45 – 10 MeV (left) and 45 – 4.5 MeV (right), are shown in relation to the onset delay duration of 45 MeV protons with respect to the type-III

radio burst. All data and errors included in this figure are taken from Table 1 of Posner, Richardson & Strauss (2024). The three events that were also MGLEs in Table 1 are labeled.

Unlike the data PRS24 is based on, the observations by RAD on the Martian surface don't allow us to undertake a meaningful estimation of MGLE energy dispersion durations for all MGLEs. Most MGLEs do not provide significant numbers of ~200 – 300 MeV primary protons that stop in the RAD detector (Hassler et al., 2018). Only the most intense events, presumably MGLEs 6 – 10, may support a partial study by applying a method to derive original proton energies at the top of the Martian atmosphere from energy loss signals of stopping protons in the RAD detector stack as described in Ehresmann et al (2017, 2018). Based on the discussion of Figure 4, and on the assumption that cross-field diffusion is responsible for spreading particles in solar longitude, we qualitatively predict long-duration ~300 MeV – 200 MeV proton energy dispersion for MGLE #6 (with a 170° magnetic connection distance) and short durations for MGLEs 8 – 10 (all with <20° absolute magnetic connection distances), while MGLE 7 (with ~60° magnetic connection distance) would be expected to have an intermediate energy dispersion duration. The dataset is not yet available to the public and the analysis is beyond the scope of this paper and may be independently tested.

We can apply a simplified test the SEP clock picture with all MGLEs by limiting ourselves to onset delays and dependency on (or lack thereof) magnetic connection distance. For this purpose, we show information on these parameters from Table 1 in Figure 5, left. As shown in Figure 4, the SEP onset delay at 45 MeV is highly correlated with energy dispersion duration. We predict that energy dispersion durations in MGLEs will likely show the same behavior, i.e., their onset delay is positively correlated with MGLE proton energy dispersion duration. Moving beyond the onset, Figure 5, right-hand side, shows a positive correlation between magnetic connection distance and peak dose rate delay. Both observed dependencies, MGLE onset- and peak delay, can also be interpreted as cross-field diffusion driving the unfolding of the event from the solar source longitude towards Mars.

We use the color coding to test whether peak dose rate has any influence on the dependencies. Overall, this seems not to be the case. We point out, however, that MGLE #11 is quite faint and its solar source association is ambiguous. The association to a source region at W21 as viewed from Mars from AR13767, and its bright type-III radio burst with SRT 1329UT) appears obvious. However, this would lead to a negative onset delay (Figure 5, left). Close inspection of the STEREO A radio data shows an earlier type-III radio burst with SRT ~1240UT that may point to a source on the far side of the Sun as viewed from STEREO-A and Earth. Such a location may be closer to the nominal magnetic connection of Mars than AR13767 is. However, as neither flare nor CME observations have been reported, for now we will maintain the association with the brighter type-III radio burst.

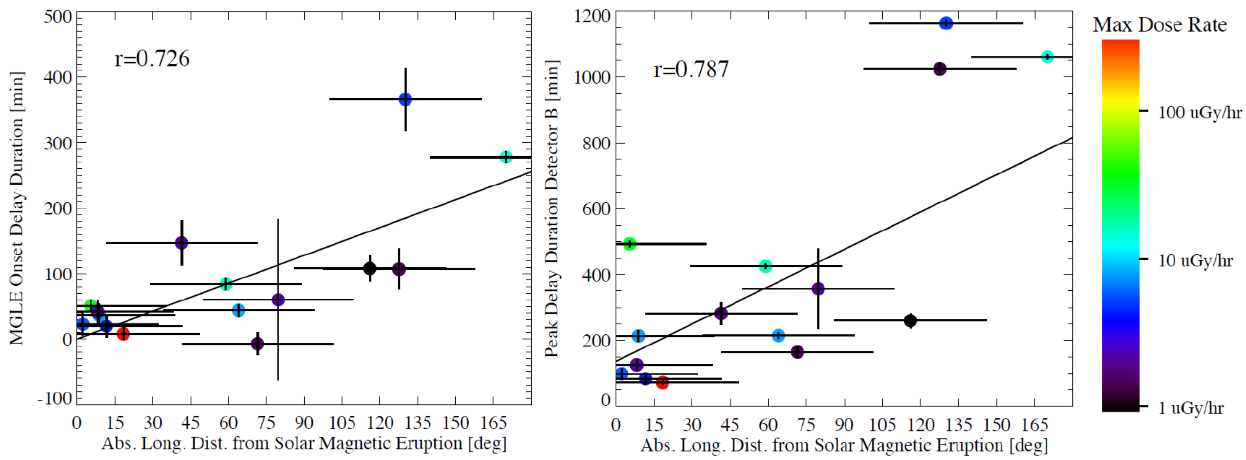

Figure 5: The figure displays onset delays (left) and peak dose rate delays (right, for detector "B") vs the magnetic connection distance inferred for each of the 15 Mars Ground Level Enhancements. The color scale identifies the peak dose rate for each event. All data and error bars are taken from Table 1.

While we fitted both the onset and peak delays with straight lines, it is more likely that the cross-field diffusion process unfolds faster where proton intensity gradients across solar/heliospheric longitudes are large. The process then slows down as the gradients decrease. This is discussed in PRS24, pointing back to the observations shown in Richardson et al., (2014, their Figure 11). A fit that rises slowly at small magnetic connection distances, but increases at larger distances, would indeed match our observations better.

Also discussed in PRS24 is that the structure of the solar wind is complex and constantly changing as the Sun expels coronal mass ejections, and corotating interaction regions and rarefactions form from the interaction of fast and slow solar wind. The magnetic sector structure, related to the heliospheric current sheet which may be flat or tilted, is also variable. All these structures can influence the propagation of SEPs and affect the rate of cross-field diffusion. Additionally, switchbacks in the inner heliosphere, which have been recently characterized using Parker Solar Probe observations, introduce another variable, as high-energy charged particles can find ways to "surf" across solar longitudes where magnetic fields are folded back on themselves. Malara et al. (2023) found by modeling that pitch angles of particles in switchback fields in the proton energy range between 1 MeV and a few GeV may be most affected. Therefore, while there are clear overall cross-field diffusion signatures, significant variability from event to event that are separated by months or years from each other should be expected, likely contributing to the observed large scatter. On the other hand, it is more likely that changes in heliospheric charged particle transport conditions are smaller on much shorter time scales of minutes to hours during the onsets of individual events. Our Figure 6 gives credence to this assumption since the displayed onset delay vs peak delay distributions of all MGLEs are highly correlated.

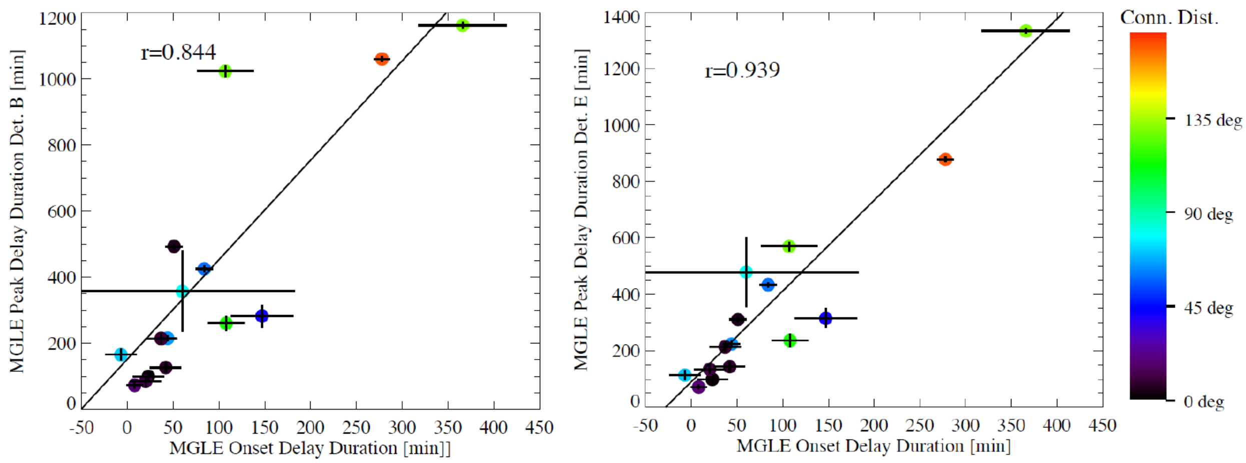

Figure 6: Onset vs peak delays for the 15 Mars Ground Level enhancements. The left-hand side uses as the peak delay that of detector "B", whereas the right-hand side uses peak delays in detector "E".

4 Mars Ground Level Enhancement Forecasting with In-Situ and Remote Sensing Instrumentation – Obstacles and Opportunities

Mars Ground Level enhancements so far have not reached intensity levels of concern for human exploration of the Martian surface. Even the highest dose rate of May 20, 2024, MGLE #9, is more than two orders of magnitude below threshold levels for acute radiation sickness. Nonetheless, reduction in dose rate for such events is still useful to keep radiation exposure as low as reasonably achievable (ALARA). This study reveals two new insights in terms of advance warning of radiation events:

4.1 A Shift in Mars Magnetic Connectivity

A simple calculation shown in Posner et al. (2021) for the Mars distance range, folding in the likelihood of 1 AU solar wind speeds to occur (Li, Zhanng & Feng, 2016), finds that the most likely magnetic field connection from Mars is near the Sun's western limb, i.e., at or near clock angle "3". Our Table 2 updates this earlier result with the solar wind speed distribution observed by MAVEN in Mars orbit as analyzed with the method described in Halekas et al. (2017). Direct observations of solar wind speeds from upstream portions of the MAVEN orbit include the time frame 2014 – 2023. Without going into detail regarding differences between 1 AU and Mars-distance solar wind parameters, we find a clear shift towards slower solar wind speeds at Mars distances. presumably because dynamic interactions between slow (dense) and fast (less dense) solar wind streams beyond 1 AU tend to erode the higher speed regions (e.g., Gosling, Hundhausen and Bame, 1976). This slow-down out at Mars semimajor axis distances around 1.5 AU nominally limits the percentage of Mars' magnetic foot point periods on the visible side of the Sun to under 35%, meaning that almost 2/3 of the time Mars would be connected with regions of the Sun that are behind the solar west limb. This is down from previous assumptions of~53% that was based on the same solar wind speed distribution as seen at 1 AU. However, if the cause of this change is dynamic interaction between 1 and 1.5 AU, one can assume that inside 1 AU the assumption of a nominal Parker spiral at slightly higher wind speeds would apply. This would shift a fraction of magnetic field connections back slightly towards the visible side of the Sun. We therefore regard both solar wind speed distributions, 1 AU and 1.5 AU, as the extreme bounds of the actual distribution that determines where Mars is connected to at the Sun.

Whitman et al. (2022) give a summary of SEP forecasting methods for the Earth-Moon system, including long-term (pre-eruption) and post-eruption techniques. Their Table 10 show that most techniques rely on direct observations of the SEP source region with remote sensing. As available (real-time) observations are mostly limited to the Sun-Earth line, important inputs of still well-connected sources are hidden from view, predominantly near or behind the W limb as viewed from Earth, where about 25% of all SEPs at 1 AU originate from (Richardson et al., 2014). This issue affects the probability of detection and false alarm rate of many SEP forecasting techniques.

Posner et al. (2021) speculate that SEP forecasting for Mars would be problematic as source regions affecting the Mars environment are frequently hidden from view of a Mars-based observer. Our new analysis of magnetic connectivity exacerbates the issue by pushing the direct magnetic connection point further west, and behind the limb . We can now confirm that SEP forecasting driven by Mars-based solar remote sensing would indeed be very ineffective. Four of 15 MGLEs, or ~27%, originate from the solar far side as viewed from Mars. Three additional MGLEs (20%) originate within 3° of the solar limb, where X-ray flares may be directly observed but solar magnetographic methods are ineffective. Thus, remote sensing of the Sun with X ray or polarimetric instrumentation from a Mars-Sun line location would be significantly more ineffective in forecasting SEPs at Mars than previously thought.

Table 2. Solar wind speed distributions at Earth and Mars and their magnetic connection longitudes. This table is adapted from Posner et al. (2021) with added MAVEN solar wind speed distributions that are based on Halekas et al. (2017).

Solar Wind Speed	**Earth**	**Mars Semim. Axis Dist**	**Mars Perihelion**	**Mars Aphelion**	**Likelihood 1 AU**	**Likelihood Mars**
275 – 325 km/s	81.8W	**124.7W**	**113.0W**	**136.3W**	8%	15%
325 – 375 km/s	70.1W	**106.9W**	**96.8W**	**116.8W**	22%	28%
375 – 425 km/s	61.4W	**93.5W**	84.7W	**102.2W**	23%	22%
425 – 475 km/s	54.5W	83.1W	75.3W	**90.9W**	16%	15%
475 – 525 km/s	49.1W	74.8W	67.8W	81.8W	11%	10%
525 – 575 km/s	44.6W	68.0W	61.6W	74.3W	7%	6%
575 – 625 km/s	40.9W	62.3W	56.5W	68.1W	5%	2%
625 – 675 km/s	37.8W	57.5W	52.1W	62.9W	4%	1%
675 – 725 km/s	35.1W	53.4W	48.4W	58.4W	3%	0.2%
725 – 775 km/s	32.7W	49.9W	45.2W	54.5W	1%	0.1%
775 – 825 km/s	30.7W	46.8W	42.4W	51.1W	<0.5%	<0.1%

4.2 Solar Radio and Mars Surface Precursors

While remote-sensing techniques that support SEP and MGLE forecasting at Mars may be ineffective, we introduce alternative means of post-eruption forecasting to be plausible and potentially quite accurate. Energetic electrons that are a reliable precursor of SEPs at 1 AU could be used for this purpose, as discussed in Posner and Strauss (2020). Type-III radio bursts appear to be reliably visible before any SEP and MGLE onset. The example of HESPERIA REleASE+ (Posner et al., 2024) shows a plausible combination of inputs in a SEP forecasting system from a Mars-Sun L1 vantage point or Mars orbit (see, e.g., Lee et al., 2023).

Noteworthy is also the predictability of the time of peak intensity of MGLEs. For this, the onset delay in RAD's detector E over the type-III radio burst can be used as a proxy. Our empirical formula for MGLE peak time past type-III onset is:

(1) Delay T_{peak}=91min + 3.2 * Delay T_{onset}

An ideal instrument installed on the Martian surface should be sensitive to both charged and neutral ionizing radiation with sufficient sensitivity to run continuously at resolution of 1-2 min. Basically, RAD matches these capabilities and runs at a baseline resolution of 1min, while switching to "SEP" mode with dosimetry data at 30sec resolution, but the high-resolution data is not yet publicly available.

After determining the time of peak dose rate, a simple extrapolation of the dose rate rise between onset and a time ΔT shortly thereafter can also give an indication of the upper bound of the expected peak dose rate:

(2) $I_{peak} = I_0$ + Delay T_{peak} * $(I_{(t1)}-I_0)/ \Delta T$

Please note that in some cases this upper bound can be orders of magnitude higher than actually observed. His is because MGLE profiles from regions not well connected tend to have a steep onset, but a slower rise at a later phase. Our estimate is for exponential rise of the steep phase and does not assume a more gradual rise to follow the initial increase.

In addition, as argued in Guo et al. (2019b), MGLE dose rates on the Martian surface can be forecasted based on the pivot-energy 300 MeV measured flux above the Martian atmosphere.

5 Summary and Conclusions

We have analyzed all 15 Mars Ground Level enhancements observed by Curiosity RAD that were observed between 2012 and the end of 2024. We have identified the solar sources that gave rise to MGLEs and placed these Mars surface particle events in context with findings of a related study of wide-spread solar particle events at 1 AU by Posner, Richardson & Strauss (2024), our main results are:

(1) The May 20, 2024 ground level enhancement serves as a good proxy for a worst-case MGLE given the extreme brightness of the associated X-ray flare, good magnetic connection conditions between active region and Mars, and Mars being near perihelion distance. The peak dose rate of this event on the Martian surface, 352 µGy/hr, while not negligible, is about two orders of magnitude below threshold levels of acute radiation effects. ALARA would apply.
(2) The most extreme percentage increase over pre-event ionizing radiation levels on Mars (May 20, 2024) is similar in magnitude to that for the GLE at Earth on Feb. 23, 1956.
(3) The ratio of ~25 MeV solar energetic proton events to MGLEs in the overlapping time period is on the order of 30 to 1.
(4) Each of the 15 MGLEs has a solar type-III radio burst precursor. This MGLE feature is also present in all STEREO-era wide-spread SEPs as defined in Posner, Richardson & Strauss (2024).
(5) Despite likely onset anisotropy, it appears that MGLE onset occurring on day- or nighttime on the surface of Mars has a negligible effect on the surface dose rate. The number of MGLE onsets at night is 8, vs. 7 at daytime.

(6) The observed distribution of solar source longitudes in clock angle relative to the longitude of Mars at 6 o'clock shows that most solar source longitudes (75%, or 9 out of 12 clock angles) have given rise to MGLEs, and we cannot rule out that the remaining longitudes (9, 10, and 11 o'clock) can also give rise to them. There is a notable clustering of solar source longitudes (4/15) in the magnetic foot point clock sector 3.

(7) Each of the MGLEs that are also included in the ~25 MeV solar proton event list by Richardson (2024) have been observed at SOHO and STEREO as proton enhancements as well, regardless their relative locations with respect to Mars or the active region source, indicating that all MGLEs cause SEPs over a wide range of solar longitudes. That would also mean that a lack of >25 MeV solar energetic proton enhancement at Earth could rule out occurrence of a MGLE.

(8) We find a positive correlation between MGLE onset time delay and magnetic connection distance. Re-analysis of the Posner, Richardson & Strauss (2024) wide-spread SEP list shows a positive correlation of onset delay and energy dispersion duration. The three MGLEs that are part of the overlapping list of events show the same pattern at 25 MeV. We predict that a) onset delay and energy dispersion duration at >180 MeV proton energies are also correlated for MGLEs and b) that magnetic connection distance and energy dispersion duration > 180 MeV are positively correlated. The latter, if confirmed, would strongly suggest that acceleration of protons to highest energies occurs very low down in the solar corona and that cross-field transport is their dominant mechanism for wide spread around the Sun. Longitudinal transport via expansion of CME shocks would give rise to an anticorrelation of magnetic connection distance and energy dispersion duration. As indicated in Ehresmann et al. (2017, 2018), MGLEs 6-10 are sufficiently intense on the Martian surface that they might be analyzed to examine the proton energy dispersion duration and test this hypothesis.

(9) We find that the delays of onset and peak of MGLEs vs the type-III radio burst solar release time are strongly correlated. This allows for a crude estimation of the time of peak dose rate, and its upper bound, adding additional tools for short-term radiation forecasting at Mars.

References

Bougeret,J. L. Kaiser, M. L., Kellogg, P. J., Manning, R., Goetz, K., et al. (1995). WAVES: The radio and plasma wave investigation on the Wind spacecraft, Spa. Sci. Rev., 71, 23, 1995. https://doi.org/10.1007/BF00751331.

Bougeret, J. L., Goetz, K., Kaiser, M. L., Bale, S. D., Kellogg, P. J., Maksimovic, M., et al. (2008). S/WAVES: The radio and plasma wave investigation on the STEREO mission. Space Science Reviews, 136(1–4), 487–528. https://doi.org/10.1007/s11214-007-9298-8.

Bruno, A., Christian, E.R., de Nolfo, G.A., Richardson, I.G., and Ryan, J.M (2019), Spectral Analysis of the September 2017 Solar Energetic Particle Events. Space Weather 17(3), 419, https://doi.org/10.1029/2018SW002085.

Dodson-Prince, H. W., Hedeman, E. R., and Mohler, O. D. (1977). Survey and comparison of solar activity and energetic particle emission in 1970, Air Force Geophysics Laboratory Techn. Rep., AFGL-TR-77-0222 1977STIN...7822013D.

Domingo, V., Fleck, B., and Poland, A. (1995). SOHO: The Solar and Heliospheric Observatory, Space Science Reviews, Volume 72, Issue 1-2, pp. 81-84, https://doi.org/10.1007/BF00768758.

Ehresmann, B., Zeitlin, C., Hassler, D. M., Wimmer-Schweingruber, R. F., Matthia, D, , Guo, J., et al. (2017). The charged particle radiation environment on Mars measured by MSL/RAD from November 15, 2015 to January 15, 2016, Life Sciences in Space Research 14, 3-11, https://doi.org/10.1016/j.lssr.2017.07.004

Ehresmann, B., Hassler, D. M., Zeitlin, C., Guo, J., Wimmer-Schweingruber, R. F., Matthiä, D., et al. (2018). Energetic particle radiation environment observed by RAD on the surface of Mars during the September 2017 event. Geophys. Res. Lett., 45, 5305–5311, https://doi.org/10.1029/2018GL077801.

Gosling, J. T., Hundhausen, A. J., and Bame, S. J. (1976). Solar wind stream evolution at large heliocentric distances: Experimental demonstration and the test of a model, J. Geophys. Res., 81, 13, htpps://doi.org/10.1029/JA081i013p02111.

Guo, J., Zeitlin, C., Wimmer-Schweingruber, R. F., Rafkin, S., Hassler, D. M., et al. (2015). Modeling the variations of dose rate measured by RAD during the first MSL Martian year: 2012-2014, Astrophys. J., 810:24, https://doi.org/0004-637X/810/1/24.

Guo, J., Dumbovic, M., Wimmer-Schweingruber, R. F., Temmer, M., Lohf, H., et al. (2018). Modeling the evolution and propagation of 10 September 2017 CMEs and SEPs arriving at Mars constrained by remote sensing and in situ measurement, Space Weather, 16, 1156–1169, https://doi.org/10.1029/2018SW001973.

Guo, J., Wimmer-Schweingruber, R. F.,Wang, Y., Grande, M., Matthiae, D., et al. (2019b). The pivot energy of solar energetic particles affecting the Martian surface radiation environment, Astrophys. J. Lett., 883:L12 (8pp),, https://doi.org/10.3847/2041-8213/ab3ec2.

Guo, J., Zeitlin, C., Wimmer-Schweingruber, R. F., Hassler, D. M., Ehresmann, B. et al (2019a). Radiation environment for future human exploration on the surface of Mars: the current understanding based on MSL/RAD dose measurements, Astron Astrophys Rev (2021) 29:8, https://doi.org/10.1007/s00159-021-00136-5(012.

Halekas, J.S., Ruhunusiri, S., Harada, Y., Collinson, G., Mitchell, D. L., Mazelle, C., McFadden, J. P., Connerney, J. E. P., Espley, J. R., Eparvier, F., Luhmann, J. G., and Jakosky, B. M. (2017). Structure, dynamics, and seasonal variability of the Mars-solar wind interaction: MAVEN Solar Wind Ion Analyzer in-flight performance and science results, J. Geophys. Res., 122, 547-578, https://doi.org/10.1002/2016JA023167.

Hassler, D. M., Zeitlin, C., Wimmer-Schweingruber, R. F., Böttcher, S., Martin, C., Andrews, J., Böhm, E., Brinza, D. E., Bullock, M. A., Burmeister, S., Ehresmann, B., Epperly, M., Grinspoon, D., Köhler, J., Kortmann, O., Neal, K., Peterson, J., Posner, A., Rafkin, S., Seimetz, L., Smith, K. D., Tyler, Y., Weigle, G., Reitz, G., and Cucinotta, F. A. (2012). The Radiation Assessment Detector investigation, Space Science Reviews, 170, 1-4, https://doi.org/10.1007/s11214-012-9913-1.

Hassler, D. M., Zeitlin, C., Wimmer-Schweingruber, R. F., Ehresmann, B., Rafkin, S., et al. (2014). Mars‘ surface radiation environment measured with the Mar Science Laboratory‘s Curiosity rover, Science, Vol. 343, https://doi.org/ 10.1126/science.1244797.

Hassler, D. M., Zeitlin, C., Ehresmann, B., Wimmer-Schweingruber, R. F., Guo, J., et al. (2018). Space Weather on the Surface of Mars: Impact of the September 2017 Events, Space Weather, 16, 1702–1708, https://doi.org/10.1029/2018SW001959.-

Jakosky, B. M., Lin, R. P., Grebowsky, J. M., Luhmann, J. G., Mitchell, D. F., Beutelschies, G., Priser, T., Acuna, M., Andersson, L., Baird, D. Baker, D., Bartlett, R., Benna,M., Bougher, S., Brain, D. Carson, D., Cauffman, S., Chamberlin, P., Chaufray, J.-Y., Cheatom, O., Clarke, J. Connerney, J., Cravens, T., Curtis, D., Delory, G., Demcak, S, DeWolfe, S. A., Eparvier, F., Ergun, R., Eriksson, A., Espley, J., Fang, X., Folta, D., Fox, J., Gomez-Rosa, C., Habenicht,S., Halekas, J., Holsclaw, G., Houghton, M., Howard, R., Jarosz, M., Jedrich, N., Johnson, M., Kasprzak, W., Kelley, M., King, T., Lankton, M., Larson, D., Leblanc, F. Lefevre, F., Lillis, R., Mahaffy, P., Mazelle, C., McClintock, W., McFadden, J., Mitchell, D. L., Montmessin, F., Morrissey, J., Peterson, W. Possel, W., JSauvaud, J.-A., Schneider, N., Sidney, W., Sparacino, S., Stewart, A. I. F., Tolson, R., Toublanc, D., Waters, C., Woods, T., Yelle R., and Zurek, R. (2015). The Mars Atmosphere and Volatile Evolution (MAVEN) Mission, Space Sci. Rev., 195, 3, https://doi.org/ 10.1007/s11214-015-0139-x\.

Javaraiah, J. (2024). Prediction of the amplitude of solar cycle 25 from the ratio of sunspot number to sunspot-group area, low latitude activity, and 130-year solar cycle, Adv. Space Res., Vol. 74, 3, 1518-1534, http://doi.org/10.1016/j.asr.2024.04.043.

Kaiser, M. L., Kucera, T. A., Davila, J., St. Cyr, O. C., Guhathakurta, M.,& Christian, E. R. (2008). The STEREO mission: An introduction. Space Science Reviews, 136(1–4), 5–16. https://doi.org/10.1007/s11214-007-9277-0

Kim, M.-H. Y., Hu, X., and Cucinotta, F. A. (2005). Effect of Shielding Materials from SPEs on the Lunar and Mars Surface, Proceedings of SPIE, 6653, https://doi.org/10.2414/6.2005-6653.

Lario, D., Richardson, I. G., Aran, A., and Wijsen, N. (2023). High-energy (>40 MeV) proton Intensity enhancements associated with the passage of interplanetary shocks at 1 au, Astrophys. J., 950 89, https://doi.org/10.3847/1538-4357/acc9c5.

Lee, C. O., Sánchez-Cano, B., DiBraccio, G. A., Mayyasi, M., Xu, S., Chamberlin, P,. Davie,s E., Scolini, C., Filwett, R. J., Ramstad, R., Palmerio, E., Lynch, B. J., Luhmann, J. G., Ehresmann, B., Guo, J., Allen, R. C., Vines, S., Winslow, R., and Elliott, H. (2023). Heliophysics and space weather science at ∼1.5 AU: Knowledge gaps and need for space weather monitors at Mars. Front. Astron. Space Sci. 10:1064208, https://doi.org/10.3389/fspas.2023.1064208.

Li, K. J., Zhanng, J., & Feng, W. (2016). A statistical analysis of 50 years of daily solar wind velocity data. The Astrophysical Journal, 151, 128. https://doi.org/10.3847/0004-6256/151/5/128.

Malara, E., Perri, S., Giacalone, J., and Zimbardo, G. (2023). Energetic particle dynamics in a simplified model of a solar wind magnetic switchback, Astron. & Astrophys. 677, A69, https://doi.org/10.1051/0004-6361/202346990.

Ogilvie, K, W., and Parks, G. K. (1996). First results from the WIND spacecraft: An introduction, Geophys. Res. Lett., Vol. 23, 10, https://doi.org/10.1029/96GL01357.

Pandey, K., Chakrabarty, D., Kumar, A., Bhardwaj, A. Biswal, S., Hussey, G. C., and Yadav, A. K. (2023). Characteristics of X-class flares of solar cycles 23 and 24 in X-ray and EUV bands, Adv. Space Res., Vol. 71, 12, 5438-5452, https://doi.org/10.1016/j.asr.2023.02.022.

Posner, A., Hassler, D. M., McComas, D. J., Rafkin, S., Wimmer-Schweingruber, R. F., Böhm, E., Böttcher, S, Burmeister, S., Dröge, W., and Heber, B. (2005). A High Energy Telescope for the Solar Orbiter, Adv. Space Res., 36, 1426-1431, https://10.1016/j.asr.2004.11.040.

Posner, A., Arge, C.N., Staub, J., StCyr, O.C., Folta, D., Solanki, S.K., Strauss, R.D.-T., Effenberger, F., Gandorfer, A., Heber, B., Henney, C.J., Hirzberger, J., Jones, S.I., Kuehl, P., Malandraki, O., Sterken, V.J.: (2021). A multipurpose Heliophysics L4 mission, Space Weather 19, 9, https://doi.org/10.1029/2021SW00277.

Posner, A., Malandraki, O. E., Karavolos, M., Tziotziou, K., Smanis, F., et al. (2024). HESPERIA REleASE+: Improving solar proton event forecasting by means of automated recognition of type-III radio bursts, Space Weather, 22,e2024SW004013. https://doi.org/10.1029/2024SW004013.

Posner, A., Richardson, I. G., Strauss, R. D.-T. (2024). The "SEP Clock": A discussion of first proton arrival times in wide-spread solar energetic particle events, Solar Physics, 299:126, https://doi.org/10.1007/s11207-024-02350-7.

Posner, A., and Strauss, R. D.-T. (2020). Warning time analysis from SEP simulations of a two-tier REleASESystem applied to Mars exploration. Space Weather, 18, e2019SW002354, https://doi.org/10.1029/2019SW002354.

Rafkin, S. C. R., C. Zeitlin, C., Ehresmann, B., Hassler, D. M., Guo, J., Köhler, J., Wimmer-Schweingruber, R. F., Gomez-Elvira, J., Kahanpää, H., Brinza, D. E., Weigle, G., Böttcher, S., Böhm, E., Burmeister, S., Martin, C.,Reitz, G.,, Cucinotta, F. A., Kim, M.-H., Grinspoon, D., Bullock, M. A., Posner, A., and the MSL Science Team, Diurnal variations of energetic particle radiation at the surface of Mars as observed by the Mars Science Laboratory Radiation Assessment Detector, J. Geophys. Res., Planets, 119, 1345–1358, doi:10.1002/2013JE004525.

Richardson, I.G., von Rosenvinge, T.T., Cane, H.V., Christian, E.R., Cohen, C.M.S., Labrador, A.W., Leske, R.A., Mewaldt, R.A., Wiedenbeck, M.E., Stone, E.C. (2014). >25 MeV Proton Events Observed by the High Energy Telescopes on the STEREO A and B Spacecraft and/or at Earth During the First ~Seven Years of the STEREO Mission, Solar Phys., 289, 3059, https://doi.org/10.1007/s11207-014-0524-8.

Richardson, I.G. (2024). Solar energetic particle events including ~ 25 MeV protons observed at STEREO and/or Earth since 2006, Harvard Dataverse V1,UNF:6:wDWbJQnOrrFoBOAs1wiZDw== [fileUNF], https://doi.org/10.7910/DVN/GQPCXZ

Van Hollebeke, M. A. I., Ma Sung, L. S., , and McDonald, F. B. (1975).The variation of solar proton energy spectra and size distribution with heliolongitude, Sol. Phys., 41, 189—223, https://doi.org/10.1007/BF00152967.

Whitman, K., Egeland, R., Richardson, I.G., Allison, C., Quinn, P., Barzilla, J., Kitiashvili, I., Sadykov, V., Bain, H.M., Dierckxsens, M., Leila Mays, M., Tadesse, T., Lee, K.T., Semones, E., Luhmann, J.G., Nú ñez, M., White, S.M., Kahler, S.W., Ling, A.G., Smart, D.F., Shea, M.A., Tenishev, V., Boubrahimi, S.F., Aydin, B., Martens, P., Angryk, R., Marsh, M.S., Dalla, S., Crosby, N., Schwadron, N.A., Kozarev, K., Gorby, M., Young, M.A., Laurenza, M., Cliver, E.W., Alberti, T., Stumpo, M., Benella, S., Papaioannou, A., Anastasiadis, A., Sandberg, I., Georgoulis, M.K., Ji, A., Kempton, D., Pandey, C., Li, G., Hu, J., Zank, G.P., Lavasa, E., Giannopoulos, G., Falconer, D., Kadadi, Y., Fernandes, I., Dayeh, M.A., Muñoz-Jaramillo, A., Chatterjee, S., Moreland, K.D., Sokolov, I.V., Roussev, I.I., Taktakishvili, A., Effenberger, F., Gombosi, T., Huang, Z., Zhao, L., Wijsen, N., Aran, A., Poedts, S., Kouloumvakos, A., Paassilita, M., Vainio, R., Belov, A., Eroshenko, E.A., Abunina, M.A., Abunin, A.A., Balch, C.C., Malandraki, O., Karavolos, M., Heber, B., Labrenz, J., Kühl, P., Kosovichev, A.G., Oria, V., Nita, G.M., Illarionov, E., O'Keefe, P.M., Jiang, Y., Fereira, S.H., Ali, A., Paouris, E., Aminalragia-Giamini, S., Jiggens, P., Jin, M., Lee, C.O., Palmerio, E., Bruno,- A., Kasapis, S., Wang, X., Chen, Y., Sanahuja, B., Lario, D., Jacobs, C., Strauss, D.T., Steyn, R., den Berg, J. van, Swalwell, B., Waterfall, C., Nedal, M., Miteva, R., Dechev, M., Zucca, P., Engell, A., Maze, B., Farmer, H., Kerber, T., Barnett, B., Loomis, J., Grey, N., Thompson, B.J., Linker, J.A., Caplan, R.M., Downs, C., Török, T., Lionello, R., Titov, V., Zhang, M., Hosseinzadeh, P. (2022). Review of Solar Energetic Particle Models, Adv. Space Res., 72, 12, doi: https://doi.org/10.1016/j.asr.2022.08.006

Wijsen, N., Aran, A., Scolini, C., Lario, D., Afanasiev, A., Vainio, R., Sanahuja, B., Pomoell, J., and Poedts, S. (2022). Observation-based modelling of the energetic storm particle event of 14 July 2012, Astron. & Astrophys., 659, A187, doi:10.1051/0004-6361/20214698.

Zeitlin, C., Hassler, D. M., Guo, J., Ehresmann, B., Wimmer-Schweingruber, R. F., et al. (2018). Analysis of the radiation hazard observed by RAD on the surface of Mars during the September 2017 solar particle event, Geophys. Res. Lett., 45, 12, https://doi.org/10.1029/2018GL077760.